Science Bulletin 65 (2020) 267–271

Contents lists available at ScienceDirect

Science Bulletin

journal homepage: www.elsevier.com/locate/scib

Short Communication

East Asia VLBI Network observations of the TeV Gamma-Ray Burst 190114C

Tao An [a,h,*], Om Sharan Salafia [c], Yingkang Zhang [a,b], Giancarlo Ghirlanda [c], Gabriele Giovannini [d,e], Marcello Giroletti [d], Kazuhiro Hada [f], Giulia Migliori [d,e], Monica Orienti [d], Bong Won Sohn [g]

[a] Shanghai Astronomical Observatory, Chinese Academy of Sciences, Shanghai 200030, China
[b] University of Chinese Academy of Sciences, Beijing 100049, China
[c] Osserv Astron Brera, Ist Nazl Astrofis, Via E Bianchi 46, Merate I23807, Italy
[d] Ist Nazl Astrofis, Ist Radioastron, Bologna I40129, Italy
[e] Department of Physics and Astronomy, University of Bologna, Bologna I40129, Italy
[f] National Astronomical Observatory of Japan, Tokyo 181-8588, Japan
[g] Korea Astronomy and Space Science Institute, Daejeon 34055, Republic of Korea
[h] Key laboratory of Radio Astronomy, Chinese Academy of Sciences, Nanjing 210008, China

ARTICLE INFO

Article history:
Received 25 August 2019
Received in revised form 18 October 2019
Accepted 6 November 2019
Available online 20 November 2019

Long duration gamma-ray bursts (GRBs) signpost the death of massive stars and the formation of stellar mass black holes (BHs). GRB emission extends from the γ-rays (the short-lived prompt emission) through the X-rays and optical/near infrared to the radio bands (the long-lived afterglow emission, reviewed in previous works [1–3]). Very high energy (VHE, $E \gtrsim 100$ GeV) emission from GRB afterglows has been long predicted (e.g., [4–6]). VHE detections provide rich information on GRB shock physics and on the conditions of the emitting zone [7]. In particular, the detection of the inverse Compton emission component would constrain the characteristic energy of the shock accelerated electrons responsible for the synchrotron emission and the fraction of the outflow kinetic energy distributed among relativistic particles and, through its amplification, magnetic field. On the other hand, the detection of VHE emission from GRBs is very challenging due to the attenuation by extra-galactic background light and/or by internal absorption. Despite that hundreds of GRBs have been detected with an afterglow, no emission at tera electron Volt (TeV) photon energy has ever been detected above 3σ [8,9] until only recently. On 14 January 2019 at UT 20:57:03, the Burst Alert Telescope (BAT) onboard NASA's Neil Gehrels *Swift* Observatory (*Swift* hereafter) detected a bright gamma-ray burst (GRB 190114C) [10]. After 50 s, this GRB was detected by the MAGIC telescope at very high energy (>300 GeV) [11] with a significance of $> 20\sigma$. The burst has been also detected by the Gamma-Ray Burst Monitor (GBM) [12] and the Large Area Telescope (LAT) [13] onboard the *Fermi* satellite. Prompt follow-up by *Swift* revealed a bright X-ray afterglow and initiated a series of multi-band follow-up observations ranging from X-ray to radio bands.

Other than being the first GRB ever to be detected by ground-based Cherenkov telescopes, GRB 190114C is a notable target of particular attraction for a number of other reasons. First, GRB 190114C shows evidence of a very early afterglow onset [14], allowing for an estimate of its initial bulk Lorentz factor (see also Ref. [15]). Second, GRB 190114C was observed and detected across 16 orders of magnitude in frequency, from γ-rays to radio, within several hours after the burst (see above paragraph), allowing for a study of the multi-band evolution of the afterglow starting early after the trigger (e.g., for a notable example of how important broadband afterglow modelling can be for the interpretation of this kind of events [16]). Third, GRB 190114C is one of the few GRBs with an early radio detection: 3.2 h after the burst it was observed by the Atacama Large Millimeter/Submillimeter Array (ALMA) at 90 GHz, revealing a fading mm-wavelength counterpart [17]; 4.2 h after the burst by the Karl G. Jansky Very Large Array (VLA) at a central frequency of 33.5 GHz [18] with a flux density of 3.1 mJy at the position of RA (J2000) = 03h38m01s.191, Dec (J2000) = $-26°56'46''.72$; later ATCA detected the source at 5.5, 9, 17 and 19 GHz with a flux density of $\sim$2 mJy about 1.5 days after the burst [19]. A detection was also reported by the RT-22 telescope, with a flux density of $\sim$4 mJy at 36.8 GHz on 2019 January 15 and 16 [20].

Fundamental information about GRB jets can be derived from radio observations of their afterglow, including jet energy, inter-

* Corresponding author.
E-mail address: antao@shao.ac.cn (T. An).

https://doi.org/10.1016/j.scib.2019.11.012
2095-9273/

stellar medium (ISM) density, and shock parameters [21]. Very Long Baseline Interferometry (VLBI), owing to its unparalleled high resolution, has been proven to be capable of providing unique information on the shock energy (and its distribution) and expansion velocity. One such case was the famous and exceptionally bright GRB 030329. Very Long Baseline Array (VLBA) and global VLBI observations determined the accurate size and source expansion velocity of GRB 030329 [22–25]. Later on, VLBI observations of GRB 170817A (the electromagnetic counterpart of the gravitational wave event GW 170817) revealed a proper motion of the radio centroid and secured constraints on its linear size at milliarcsecond scales, invaluable in telling competing models for the ejecta dynamics apart [26–28]. Modelling the temporal evolution of radio flux densities offers critical constraints on the progenitor environment. The multi-band light curves of the extremely bright GRB 130427A can be described by a two-jet model, which favors a low-density progenitor environment [29–31].

Multi-epoch European VLBI Network (EVN) and VLBA observations of GRB 151027A played a pivotal role in favouring the wind density profile model, typical of the medium surrounding a massive star in the final stages of its evolution, rather than a homogeneous profile typical of the interstellar medium [32]. Given the exceptional brightness and energy spectrum of GRB 190114C, this seemed another ideal case to take advantage of high angular resolution and sensitivity provided by the VLBI technique.

Owing to the above reasons, we applied for VLBI observations of GRB 190114C with the East Asia VLBI Network (EAVN) [33]. It is critical to have a proper characterisation of the emission in the first days, when it is possible to observe the source at high frequency. Moreover, multi-epoch VLBI radio observations starting in the immediate aftermath of the burst enable to determine or constrain the source expansion. In order to fulfill these described goals, we conducted VLBI observations at 22 GHz in three epochs within about one month after the burst. The VLBI observational results and insights from afterglow modelling are presented in this paper.

We carried out high-resolution follow-up observations of GRB 190114C with the East Asia VLBI Network on three epochs of 2019 January 21, 30, and 2019 February 16, which correspond to 6, 15 and 32 days respectively after the burst discovered on 2019 January 15 (see the report in Ref. [34]). These observations made use of the Director's Discretionary Time (DDT). The first observation was scheduled as soon as possible, within 1 week after the burst, with the initial purpose of constraining the self-absorption frequency. The primary purpose of the second and third epochs was to monitor the flux density evolution in order to track the possible evolution of the self-absorption frequency and, if possible, to determine or constrain the source expansion speed. They would also have the added value of validating and strengthening any positional constraints derived from the first epoch.

Altogether, eight telescopes participated in the observations. The detailed observation setup is presented in Table A1 (online). The same observation setup was used in the three sessions. Although the target is at a relatively low declination, each station could observe it at elevation $> 20^\circ$ for most of the time during the observing runs and with a maximum elevation angle up to 40°. An example of the (u,v) coverage is shown in Fig. A1 (online). The observations were carried out in phase referencing mode. The nearby bright source J0348-2749 (1.2 Jy at 22 GHz; 2.5° away from the target on the plane of the sky) was used as the calibrator. The image of J0348-2749 is displayed in Fig. B1 (online), showing a compact core-jet structure. We first calibrated the phases of J0348-2749, then applied the complex gain solutions derived from J0348-2749 to the target source data by interpolation. The data were finally averaged in frequency within each sub-band, but individual sub-bands were kept to minimize bandwidth smearing. Similarly, the data were time-averaged to 2 s for imaging. Additional details on the observation and data reduction are deferred to the Supplementary materials.

We compare the upper limits from our radio observations with standard afterglow model predictions, and we model the GRB afterglow emission following Granot and Sari [35], which accounts for synchrotron emission from electrons in a relativistic shock whose hydrodynamical profile is described by the self-similar [36] solution. The number density profile of the external medium in which the shock propagates is parametrized as $n(R) \propto R^{-k}$, where the two relevant scenarios in GRBs are $k = 0$ (constant density medium, representing a uniform ISM region) or $k = 2$ (the expected density profile of the circum-burst medium produced by the winds of the progenitor star, e.g., Ref. [37]). A fraction ϵ_e of the energy density in the shocked material is assumed to take the form of relativistic electrons (accelerated into a non–thermal energy distribution with index p), while a fraction ϵ_B is assumed to be shared by the magnetic field, amplified by small-scale magneto–hydrodynamic instabilities. These parameters suffice to derive the synchrotron emission, i.e., the spectral shape and normalization, at all times for which the underlying assumptions hold.

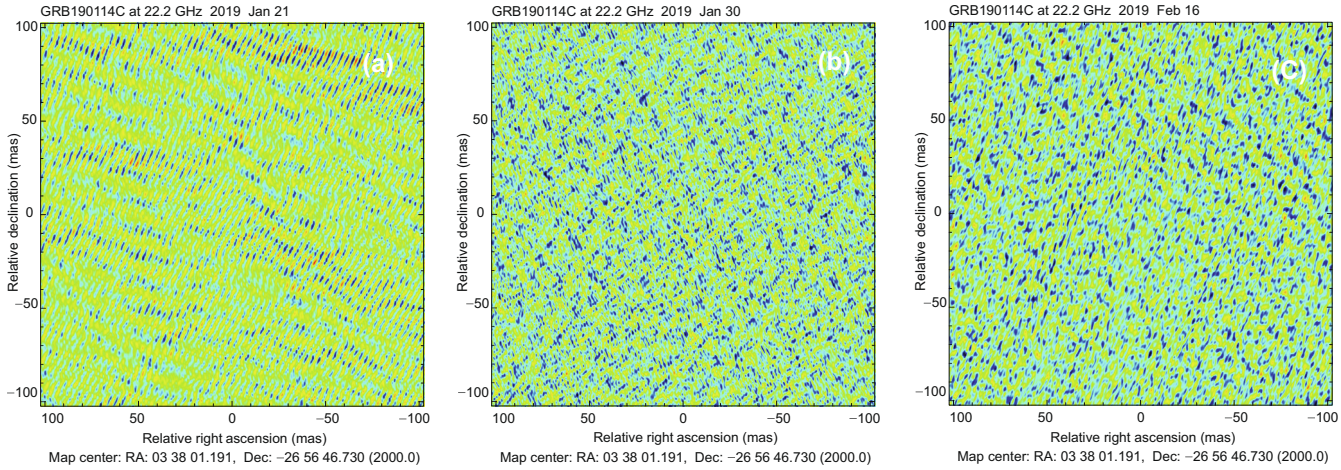

Fig. 1. (Color online) The EAVN images of the target GRB 190114C. The images are made by using natural weighting. The color scale represents the brightness: from −3.69 (dark blue color) to 4.24 (red color) mJy beam^{-1} (panel a), from −2.7 to 2.67 mJy beam^{-1} (panel b), and from −1.19 to 1.18 mJy beam^{-1} (panel c). The rms noise is 0.9, 0.6, and 0.3 mJy beam^{-1} for panels (a), (b) and (c), respectively. The image center (RA = 03h38m01s.191, Dec = −26°56′46″.730) was adopted from the VLA observation [18]. There is no significant source brighter than 5σ in the 200 mas × 200 mas field.

Fig. 1 shows the images of the sky zone. The root mean square (rms) noise in the three images is 0.92, 0.61 and 0.28 mJy beam^{-1}, respectively (Table B1 online). As a comparison, the image noise derived from the Korean and Japanese-only telescopes results in an increase by 28%–45%. The first epoch has only five telescopes, compared to seven telescopes in other two sessions, and thus has a relatively higher noise level. The images cover a square region of the sky, with a side length of 200 mas, centered at RA = 03h38m01s.191, Dec = −26°56′46″.730 (J2000), i.e., the same as the position determined from the VLA observation [18]. The positional uncertainty given by the VLA observation is 0.04″ in RA direction and 0.02″ in Dec direction, respectively. Therefore a field with a radius of 100 mas is large enough to search for the GRB signal. An integration time of 1 s was used in correlation, to avoid time smearing effects. There is no significant peak brighter than 5σ in either image. Fig. 1a displays ripples in which there are some bright points with a maximum brightness of $\sim 4\sigma$. The ripples are caused by sparse sampling of the visibilities resulted from a limited number of telescopes (five, corresponding to 10 geographical baselines). These 4σ points do not have corresponding counterparts in Fig. 1b and c, whose noise level is 1.5–3 times lower. Therefore we regard these peaks as noise. In contrast, Fig. 1b and c show a smooth field without any clues of dominant signals which can be identified as candidate sources. In conclusion, we did not detect GRB 190114C from the EAVN data in the three epochs. A 3σ upper limit is given as 2.76 mJy (2019 January 21), 1.82 mJy (2019 January 30) and 0.84 mJy (2019 February 16) respectively and used to constrain the model parameters below.

The afterglow of GRB 190114C has been studied in a number of recent works, some of which are still in preprint form, while others have been published. Wang et al. [38] model the multi-wavelength emission after ~1ks as synchrotron radiation from the forward shock. A similar modelling is proposed by Fraija et al. [39], where the early optical/X-ray emission is instead interpreted as due to the deceleration of the jet in a wind-like stratified medium. The radio (1.3–97 GHz) emission in the early phase up to ~1ks has been interpreted as due to the emission by the transient reverse shock that marks the time during which the jet injects its energy into the shocked region [40]. At present two possible scenarios seem to emerge in the interpretation of the available multi-

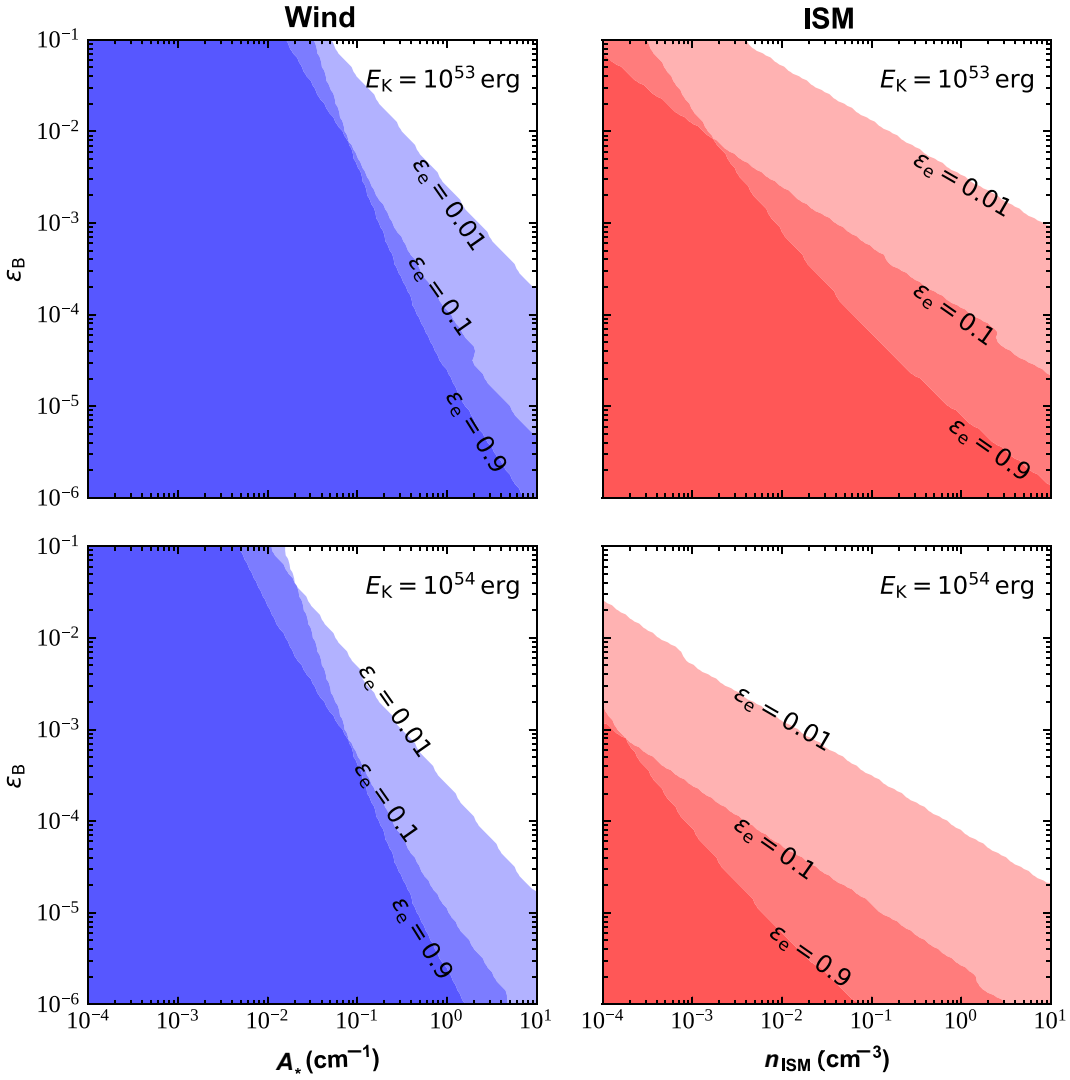

Fig. 2. (Color online) Constraints on the forward shock synchrontron afterglow model parameters. The panels show either the 2D parameter space ϵ_B–A_* (for the wind external medium – left-hand column) or ϵ_B–n_{ISM} (for the uniform ISM external medium – right-hand column). The parameter A_* is the density parameter for the wind medium (as defined in Ref. [37]). Coloured regions correspond to parameters that produce radio emission consistent with our upper limits. Each plot shows three shaded regions corresponding to three different values of ϵ_e, namely 0.01, 0.1 and 0.9. The two rows correspond to two possible values of the outflow kinetic energy, namely $E_k = 10^{53}$ erg and 10^{54} erg.

wavelength data: either emission from the reverse/forward shock component in a wind medium (where the reverse and forward shock emission dominate the early- and late-time emission, respectively) or emission dominated solely by the forward shock produced by the expansion of the outflow in a medium whose density evolves from a wind environment to an ISM with a constant number density [39].

These different scenarios will be best tested by considering all the available multi-wavelength data sets. In particular the TeV data by MAGIC can constrain the fraction of energy of the electrons ϵ_e along with other afterglow parameters (see e.g., Ref. [7]). Here we show to what extent our three radio observations can constrain the parameter space of a standard forward shock synchrotron afterglow model (given that, at our observation time, any reverse shock contribution would not be relevant anymore). We consider the two possible external medium scenarios (ISM or wind) and three possible values of the parameter $\epsilon_e = [0.01, 0.1, 0.9]$ which correspond to the range of values adopted to model this afterglow in the literature. The afterglow flux is governed, among other parameters, by the outflow kinetic energy: we consider two possible values $E_k = [10^{53}, 10^{54}]$ erg. Considering the isotropic equivalent energy radiated in γ-rays of $\sim 3 \times 10^{53}$ erg as measured from the prompt emission spectrum (e.g., Ref. [14]), the assumed values for E_k correspond to an efficiency of the prompt phase ($\eta \sim E_{\gamma,iso}/E_k$) of 75% and 30%, respectively. Finally, we assume a typical spectral index of the electron power-law distribution $p = 2.3$ (this parameter has little impact on the emission at our frequencies). With these assumptions, we explore the parameter space given by the combination of the energy in the magnetic field, described through parameter ϵ_B, and the density of the external medium n (or the normalization of the wind profile A_*) and require the afterglow emission at 6, 15 and 32 days at 22 GHz to be consistent with our upper limits. In Fig. 2 we show the parameter space allowed by our three upper limits with colored regions for the possible combinations of the assumed parameter values described above. Each shade of colour refers to a different value of ϵ_e; the two rows refer to the two considered values of isotropic-equivalent kinetic energy E_k; the two columns refer to the wind (left-hand column) and uniform ISM (right-hand column) cases. Additionally, in Fig. 3 we compare our limits with the expected 22 GHz emission for the various parameter sets proposed so far in the literature. Most parameter values are consistent with our upper limits.

We carried out follow-up observations of GRB 190114C with the EAVN at 22 GHz in three epochs, on 6, 15 and 32 days after the burst respectively. In none of the images derived from the three VLBI observations we find a source with brightness above 5σ, suggesting that the source flux density has rapidly declined. The present observations set upper limits of radio emission of GRB 190114C, offering useful constraints on the parameter space (e.g., energy fraction of the magnetic field, density of external medium, kinetic energy) of the synchrotron afterglow model of a standard forward shock. The modelled light curves in the recent papers are found to be consistent with our upper limits.

In addition to its scientific importance, this observation campaign is of particular merit: it is the first time for the EAVN to conduct fast-response observations of a transient. The experience gained, i.e., completion of the sequence of proposing the observations, coordinating the efforts at the various stations, scheduling and conducting the first-epoch observation within one week after the X-ray triggering, is very useful for a future Target-of-Opportunity (ToO) operational mode of the EAVN. Moreover, this is the first phase-referencing observation of the EAVN. So far, the EAVN has mostly been limited to the observations of bright sources (e.g., [41–43]), therefore the capability of phase referencing will greatly expand its science applications.

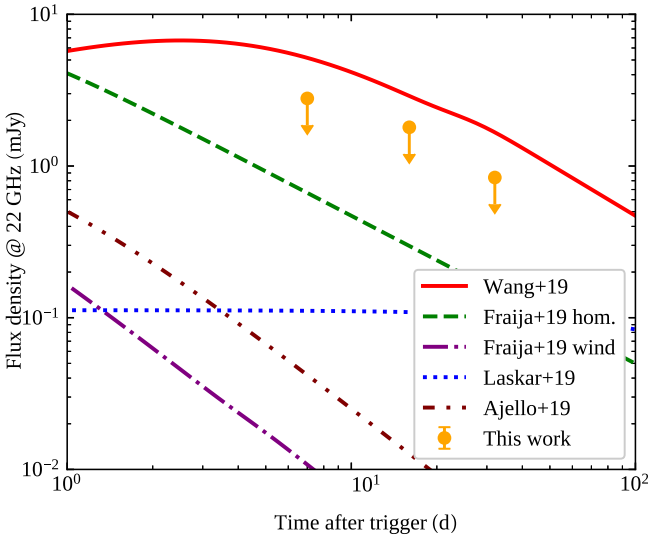

Fig. 3. (Color online) Comparison of our upper limits with the expected 22 GHz afterglow light curves for different models proposed in the literature. The three orange circles with downward arrows represent our three-sigma upper limits. Each line represents the expected 22 GHz afterglow light curve for a different set of parameters, computed following Ref. [35]. The sets of parameters correspond to those used in a number of recent papers that model the GRB 190114C afterglow, as reported in the legend. The parameters of Ref. [38] are excluded by our observations.

Conflict of interest

The authors declare that they have no conflict of interest.

Acknowledgments

We acknowledge the financial support by the National Key R&D Programme of China (2018YFA0404603), PRIN-INAF 2016, Korea's National Research Council of Science & Technology (NST) granted by the International Joint Research Project (EU-16-001). T.A. thanks the grant support from the Youth Innovation Promotion Association of CAS. We are grateful to the EAVN Directors, the scheduler, and the staff at the stations and at the KJCC for making the observations into reality. We also thank Lara Nava and Maria Edvige Ravasio for their helpful discussion and constructive comments on the manuscript.

Author contributions

Tao An and Marcello Giroletti coordinated the observation. Tao An, Om Salafia and Giancarlo Ghirlanda drafted and revised the paper. Yingkang Zhang, Marcello Giroletti and Kazuhiro Hada analyzed the VLBI Data. Om Salafia and Giancarlo Ghirlanda made the afterglow model. All authors contributed to the observation design and the discussion and interpretation of the data.

Appendix A. Supplementary materials

Supplementary materials to this article can be found online at https://doi.org/10.1016/j.scib.2019.11.012.

References

[1] Fishman GJ, Meegan CA. Gamma-ray bursts. Annu Rev Astron Astrophys 1995;33:415–58.
[2] van Paradijs J, Kouveliotou C, Wijers RAMJ. Gamma-ray burst afterglows. Annu Rev Astron Astrophys 2000;38:379–425.

[3] Piran T. Magnetic fields in gamma-ray bursts: a short overview. Am Inst Phys Conf Proc 2005;784:164–74.
[4] Chiang J, Dermer CD. Synchrotron and synchrotron self-compton emission and the blast-wave model of gamma-ray bursts. Astrophys J 1999;512:699–710.
[5] Zhang B, Mészáros P. High-energy spectral components in gamma-ray burst afterglows. Astrophys J 2001;559:110–22.
[6] Fan YZ, Piran T. High-energy γ-ray emission from gamma-ray bursts—before GLAST. Front Phys China 2008;3:306–30.
[7] Derishev E, Piran T. The physical conditions of the afterglow implied by MAGIC's sub-TeV observations of GRB 190114C. Astrophys J 2019;880:L27.
[8] Vurm I, Beloborodov AM. On the prospects of gamma-ray burst detection in the TeV Band. Astrophys J 2017;846:152.
[9] Nava L. High-energy emission from gamma-ray bursts. Int J Mod Phys D 2018;27:1842003.
[10] Gropp JD, Kennea JA, Klingler NJ, et al. GRB 190114C: swift detection of a very bright burst with a bright optical counterpart. GRB Coord Netw 2019;23688:1.
[11] Mirzoyan R, Noda K, Moretti E, et al. MAGIC detects the GRB 190114C in the TeV energy domain. GRB Coord Netw 2019;23701:1.
[12] Hamburg R, Veres P, Meegan C, et al. GRB 190114C: Fermi GBM detection. GRB Coord Netw 2019;23707:1.
[13] Kocevski D, Omodei N, Axelsson M, et al. GRB 190114C: Fermi-LAT detection. GRB Coord Netw 2019;23709:1.
[14] Ravasio ME, Oganesyan G, Salafia OS, et al. GRB 190114C: from prompt to afterglow? Astron Astrophys 2019;626:A12.
[15] Ajello M, Arimoto M, Axelsson M, et al. Fermi and swift observations of GRB 190114C: tracing the evolution of high-energy emission from prompt to afterglow. arXiv:1909.10605, 2019.
[16] Racusin JL, Karpov SV, Sokolowski M, et al. Broadband observations of the naked-eye γ-ray burst GRB080319B. Nature 2008;455:183–8.
[17] Laskar T, Alexander KD, Berger E, et al. GRB 190114C: ALMA detection of a fading mm counterpart. GRB Coord Netw 2019;23728:1.
[18] Alexander KD, Laskar T, Berger E, et al. GRB 190114C: VLA detection. GRB Coord Netw 2019;23726:1.
[19] Schulze S, Anderson G, Moin A, et al. GRB190114C: ATCA detection of the radio afterglow. GRB Coord Netw 2019;23745:1.
[20] Volvach AE, Volvach LN, Pozanenko A. GRB 190114C: RT-22 detection at 36.8 GHz. GRB Coord Netw 2019;23750:1.
[21] Granot J, van der Horst AJ. Gamma-ray burst jets and their radio observations. Publ Astron Soc Aust 2014;31:e008.
[22] Taylor GB, Frail DA, Berger E, et al. The angular size and proper motion of the afterglow of GRB 030329. Astrophys J 2004;609:L1–4.
[23] Taylor G, Frail D, Berger E, et al. High resolution radio observations of GRB 030329. Eds: Romney JD, Reid MJ. Future directions in high resolution astronomy. Astron Soc Pacific Conf Ser 2005;340:298.
[24] Pihlström YM, Taylor GB, Granot J, et al. Stirring the Embers: high-sensitivity VLBI observations of GRB 030329. Astrophys J 2007;664:411–5.
[25] Mesler RA, Pihlström YM, Taylor GB, et al. VLBI and Archival VLA and WSRT observations of the GRB 030329 radio afterglow. Astrophys J 2012;759:4.
[26] Mooley KP, Nakar E, Hotokezaka K, et al. A mildly relativistic wide-angle outflow in the neutron-star merger event GW170817. Nature 2018;554:207–10.
[27] Mooley KP, Deller AT, Gottlieb O, et al. Superluminal motion of a relativistic jet in the neutron-star merger GW170817. Nature 2018;561:355–9.
[28] Ghirlanda G, Salafia OS, Paragi Z, et al. Compact radio emission indicates a structured jet was produced by a binary neutron star merger. Science 2019;363:968–71.
[29] van der Horst AJ, Paragi Z, de Bruyn AG, et al. A comprehensive radio view of the extremely bright gamma-ray burst 130427A. Mon Not Roy Astron Soc 2014;444:3151–63.
[30] Perley DA, Perley RA, Hjorth J, et al. Connecting GRBs and ULIRGs: a sensitive, unbiased survey for radio emission from gamma-ray burst host galaxies at $0<z<2.5$). Astrophys J 2015;801:102. .
[31] Maselli A, Melandri A, Nava L, et al. GRB 130427A: a nearby ordinary monster. Science 2014;343:48–51.
[32] Nappo F, Pescalli A, Oganesyan G, et al. The 999th Swift gamma-ray burst: some like it thermal. A multiwavelength study of GRB 151027A. Astron Astrophys 2017;598:A23.
[33] An T, Sohn BW, Imai H. Capabilities and prospects of the East Asia very long baseline interferometry network. Nat Astron 2018;2:118–25.
[34] Giroletti M, Orienti M, Ghirlanda G, et al. 2019, GRB 190114C: EAVN observations at 22 GHz. GRB Coord Netw 2019;24766:1.
[35] Granot J, Sari R. The shape of spectral breaks in gamma-ray burst afterglows. Astrophys J 2002;568:820–9.
[36] Blandford RD, McKee CF. Fluid dynamics of relativistic blast waves. Phys Fluids 1976;19:1130–8.
[37] Chevalier RA, Li ZY. Wind interaction models for gamma-ray burst afterglows: the case for two types of progenitors. Astrophys J 2000;536:195–212.
[38] Wang XY, Liu RY, Zhang HM, et al. Synchrotron self-compton emission from external shocks as the origin of the sub-TeV emission in GRB 180720B and GRB 190114C. Astrophys J 2019;884:117.
[39] Fraija N, Dichiara S, Pedreira ACC do ES, et al. Analysis and modeling of the multi-wavelength observations of the luminous GRB 190114C. Astrophys J 2019;879:L26. .
[40] Laskar T, Alexander KD, Gill R, et al. ALMA detection of a linearly polarized reverse shock in GRB 190114C. Astrophys J 2019;878:L26.
[41] An T, Cui YZ, Paragi Z, et al. VLBI observations of flared optical quasar CGRaBS J0809+5341. Publ Astron Soc Jpn 2016:68–77.
[42] Hada K, Park JH, Kino M, et al. Pilot KaVA monitoring on the M 87 jet: confirming the inner jet structure and superluminal motions at sub-pc scales. Publ Astron Soc Jpn 2017;69:71.
[43] Lee T, Trippe S, Kino M, et al. Jet kinematics of the quasar 4C+21.35 from observations with the KaVA very long baseline interferometry array. Mon Not Roy Astron Soc 2019;486:2412–21.

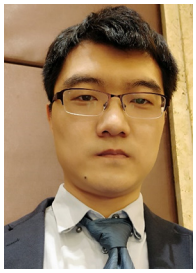

Tao An is a professor at the Shanghai Astronomical Observatory of the Chinese Academy of Sciences. He is Member of Square Kilometre Array (SKA) Regional Centre Streering Committee and International Astronomical Society (IAU) Commission B4, co-chair of SKA VLBI science working group. He is leading the China SKA Regional Centre prototype construction. His research fields are astrophysics, radio astronomy, and very long baseline interferometry (VLBI).